Deep-inelastic events containing a measured jet as a probe of QCD behavior at small x

J. Kwiecinski,* A. D. Martin, and P. J. Sutton
Department of Physics, University of Durham, Durham DH1 3LE, England
(Received 7 February 1992)

We examine the proposal that deep-inelastic (x, Q^2) scattering events which contain an identified jet, with transverse momentum squared $k^2 \simeq Q^2$, allow an ideal determination of the QCD behavior at very small x. We solve the Lipatov equation to predict the shape of the jet spectrum in such events and show that measurements at the DESY ep collider HERA should be able to verify, inter alia, whether the gluon indeed has the theoretically anticipated $g \sim x^{-\alpha_P}$ small-x behavior with the intercept α_P of the bare perturbative QCD Pomeron possibly as large as 1.5.

PACS number(s): 13.60.Hb, 12.38.Bx, 12.38.Qk, 13.87.Ce

I. INTRODUCTION

The behavior of parton distributions at small x is phenomenologically important, but is also of great theoretical interest since it illuminates the properties of QCD in a new regime. Although as $x \to 0$ we ultimately enter the nonperturbative regime of QCD, there is a transitional region in which novel theoretical ideas have been introduced to extend the applicability of perturbative QCD to smaller x than hitherto [1]. These novel effects are expected to become evident in the region $x \lesssim 10^{-2}$–10^{-3}, which will be probed by the next generation of colliders [that is, the DESY ep collider HERA, the CERN Large Hadron Collider (LHC), and the Superconducting Super Collider (SSC)]. In this small-x region the partons are mainly gluons (and sea quarks which originate from the gluons) and so we focus attention on the behavior of $g(x, Q^2)$, the gluon distribution in a proton, in the small-x, large-Q^2 region, or to be precise in the region where Q^2 is at least about a couple of GeV^2 so that QCD perturbation theory is applicable. As usual, x is the Bjorken variable,

$$x = \frac{Q^2}{2p \cdot q}, \tag{1}$$

and $Q^2 = -q^2$ where p is the four-momentum of the proton and q is the four-momentum transfer of the probe.

The traditional way to estimate the behavior of $g(x, Q^2)$ at small x and large Q^2, based on the Altarelli-Parisi (or Dokshitzer-Gribov-Lipatov-Altarelli-Parisi) evolution equations [2], is to sum the leading powers of $\ln(1/x)$ and $\ln(Q^2/\Lambda^2)$. That is for each additional factor of α_s we keep only the leading $\ln(1/x)\ln(Q^2)$ term accompanying that α_s. In axial gauges, these leading double logarithms are generated by "ladder" diagrams (Fig. 1) in which the gluons have strongly ordered transverse momenta

$$Q^2 \gg k_T^2 \gg k_{nT}^2 \gg \cdots \gg k_{1T}^2 \gg k_{0T}^2. \tag{2}$$

The sum of these diagrams gives

$$xg(x, Q^2) \propto \exp\left[2\left(\frac{3\alpha_s}{\pi}\ln(Q^2)\ln(1/x)\right)^{\frac{1}{2}}\right] \tag{3}$$

at small x and large Q^2, where we have omitted a slowly varying multiplicative $[\ln(Q^2)\ln(1/x)]^{-1/2}$ factor. If we include the running of α_s then $\alpha_s \ln(Q^2)$ becomes $\propto \ln[\ln(Q^2)]$. However, this form, (3), based on the Altarelli-Parisi equations, does not take into account all the leading terms in the small-x limit. It neglects, by definition, those terms in the perturbation expansion which contain the leading power of $\ln(1/x)$ but which are not accompanied by the leading powers of $\ln(Q^2)$. To sum the leading $\ln(1/x)$ terms we should retain the full Q^2 dependence [and relax the strong ordering of the k_T's, shown in Eq. (2), which generated the leading $\ln(Q^2)$ behavior] and integrate over the full k_T phase space with

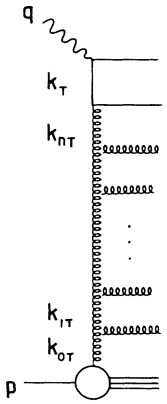

FIG. 1. Diagrammatic representation of a deep-inelastic probe of the gluon content of the proton at high Q^2. p and q are the proton and virtual photon 4-momenta, respectively, and $Q^2 = -q^2$.

*Permanent address: H. Niewodniczanski Institute of Nuclear Physics, 31-342 Krakow, Poland.

$Q^2, k_T^2, k_{nT}^2, \ldots$ only restricted to be much larger than Λ^2. The sum of these leading $\ln(1/x)$ terms is given by the Lipatov (or Balitsky-Kuraev-Fadin-Lipatov) equation [3, 4], which leads to a small-x behavior of the form

$$xg(x,Q^2) \propto x^{-\alpha_P+1} \tag{4}$$

with

$$\alpha_P - 1 = \frac{12\alpha_s}{\pi}\ln 2, \tag{5}$$

where, for simplicity, we have again neglected the effects of the running of α_s, and omitted the relatively slowly varying $[\ln(1/x)]^{-1/2}$ factor. α_P is the intercept of the bare QCD Pomeron, or so-called "Lipatov" Pomeron, and since $\alpha_P - 1 \sim 0.5$ (for a typical $\alpha_s \sim 0.2$) we should expect to see a spectacular growth of $xg(x,Q^2)$ as $x \to 0$.

Clearly the growth shown in Eq. (4) [or, for that matter, in Eq. (3)] cannot go on indefinitely with decreasing x, since eventually the density of gluons will become so large that they can no longer be treated as free partons. Recombination of gluons will begin to occur and compete with the evolution in such a way as to limit the growth of $xg(x,Q^2)$ [1, 5–9]. However there is an "intermediate" region of x, with $x \sim 10^{-3}$, where these shadowing or recombination effects are expected to be small and where the rapid "Lipatov" growth should be evident.

So far experiments have not been able to probe down to such small x values (at least for Q^2 large enough to be in the perturbative region) and so no confirmation of the Lipatov (or QCD) Pomeron exists yet. Measurements of the deep-inelastic structure functions $F_L(x,Q^2)$ and $F_2(x,Q^2)$ at HERA can probe $g(x,Q^2)$ and $\bar{q}(x,Q^2)$, respectively, in this region of x, but over a limited range of Q^2 [10]. The comparison of the experimentally determined parton distributions with the QCD predictions is complicated by the need to input some "starting" parton distributions (such as their x behavior at $Q_0^2 = 4$ GeV^2) in the QCD calculation. Thus if a steep behavior were to be observed at small x [such as in Eq. (4)] which, most reasonably, could be taken to indicate the existence of the Lipatov Pomeron, there is always the possibility that the effect could be of nonperturbative origin. A study of the Q^2 dependence would appear to be of little help. The steep behavior with decreasing x that is generated by the Lipatov equation is stable to evolution in Q^2. Moreover the Q^2 dependence arising from the Lipatov equation is similar to that given by using the Altarelli-Parisi evolution equation [7, 11–13]. Finally, only a limited range of Q^2 is accessible at HERA, for small values of x, so the evolution length $\ln(Q^2_{\max}/Q^2_{\min})$ is small; recall that $Q^2_{\min}$ has to be large enough for perturbative QCD to be valid.

It is clearly desirable to look for experiments which focus on the small-x behavior of QCD (rather than its Q^2 behavior) and which, unlike the deep-inelastic F_L and F_2 structure function measurements, do not depend on assuming some input x distribution. An intriguing proposal has been made by Mueller [14]. The idea is to study deep-inelastic (x,Q^2) events which contain an identified jet (x_j, k_{1T}^2) where $x \ll x_j$ and $Q^2 \simeq k_{1T}^2$. The process is illustrated in Fig. 2 where the jet arises from parton a

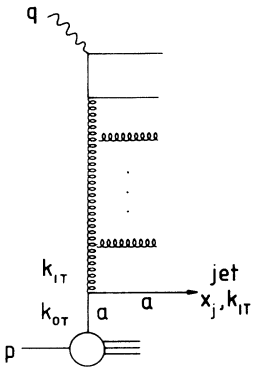

FIG. 2. Diagrammatic representation of a deep-inelastic event which contains an identified jet with longitudinal and transverse momentum of $x_j p$ and k_{1T}, respectively. x_j is chosen as large as experimentally feasible ($x_j \sim 0.1$) and so we assume strong-ordering of the longitudinal, as well as transverse, momentum at the parton a-gluon vertex. Parton a may be either a quark or a gluon.

(which can be either a quark or a gluon). The longitudinal momentum fraction x_j carried by the jet is chosen not to lie in the small-x region and the strong-ordering of transverse momenta at the gluon-a vertex ($k_{0T}^2 \ll k_{1T}^2$) means that the exchanged gluon and the jet have approximately the same transverse momentum, as shown in Fig. 2. Since we choose events with $k_{1T}^2 \simeq Q^2$ the Q^2 evolution is neutralized and attention is focused on the small-x, or rather the small-x/x_j, behavior.

It is convenient to express the rate (or cross section) of deep-inelastic events containing an identified jet as a differential structure function in terms of the jet variables, $\partial F_2/\partial x_j\, \partial k_{1T}^2$. Recalling that the Lipatov sum of the gluon emissions shown in Fig. 1 gave the behavior shown in Eq. (4), we would expect the deep-inelastic + jet events arising from Fig. 2 will have the form

$$x_j k_{1T}^2 \frac{\partial F_2}{\partial x_j\, \partial k_{1T}^2} \sim \alpha_s(k_{1T}^2)\left(x_j \sum_a f_a(x_j, k_{1T}^2)\right) \times \left(\frac{x}{x_j}\right)^{1-\alpha_P}, \tag{6}$$

where, assuming t-channel pole dominance, the sum over the parton distributions is

$$\sum_a f_a = g + \frac{4}{9}(q + \bar{q}). \tag{7}$$

The factor α_s arises in Eq. (6) because the structure function for events with an identified jet is of $O(\alpha_s)$ in relation to the inclusive deep-inelastic structure function F_2. In the next section we show that the QCD prediction has indeed just this type of behavior and so a measurement of the x/x_j dependence of deep inelastic + jet events should reveal the Lipatov Pomeron; it has been heralded as a landmark measurement of QCD [14].

We have mentioned one reason why this measurement is so special: the choice $k_{1T}^2 \simeq Q^2$ means we have eliminated the strongly ordered gluon emissions associated

with the standard Altarelli-Parisi evolution. However there is a second reason. The small x/x_j behavior of Eq. (6) is directly linked with the high-energy behavior of the virtual-photon–virtual-parton-a cross section. This is evident because the center-of-mass energy $\sqrt{s_{\gamma a}}$ of this subprocess is given by

$$s_{\gamma a} \simeq 2k_a \cdot q \simeq 2x_j p \cdot q = \left(\frac{x_j}{x}\right) Q^2,$$

using Eq. (1). Note that the four-momentum of the exchanged parton a in Fig. 2 is $k_a \simeq x_j p$ on account of the strong-ordering of the longitudinal momenta which holds at the gluon-a vertex, since x_j is $O(1)$. Thus the proposed experimental determination of the QCD small x behavior is associated with the high-energy behavior of a *partonic* cross section; as opposed to directly measuring the small-x behavior of parton distributions in a *proton* which necessarily are accompanied by nonperturbative ambiguities (in the form of assumed "starting" x distributions).

The above special features are shared by inclusive dijet production in hadronic collisions, for certain kinematic regions of the jets [15], where again the small-x behavior is associated with the high-energy behavior of a partonic subprocess. However the electroproduction of a single jet should be more accessible to experiment, particularly with the advent of HERA.

The outline of the paper is as follows. In the next section we derive the precise QCD form of the differential structure function for deep-inelastic events containing an identified jet. In the fixed coupling case we are able to obtain a closed analytic expression for $\partial F_2/\partial x_j \partial k_{1T}^2$ in the leading $\ln(x_j/x)$ approximation. We then turn to the more realistic running coupling case and describe a procedure that allows a numerical solution of the Lipatov equation. In Sec. III we implement this procedure and present numerical values of the differential structure function $\partial F_2/\partial x_j \partial k_{1T}^2$ as a function of x and x_j. These results show that the analytic (fixed coupling) approximation overestimates the rate of deep-inelastic events containing an identified jet. We discuss special features of the differential structure function and, in particular, we show how measurements of the shape of the jet spectrum can reveal the small-x behavior of QCD. In Sec. IV we give our conclusions.

II. THE CROSS SECTION FOR DEEP-INELASTIC + JET EVENTS

We are interested in the process in which deep-inelastic scattering is accompanied by a single identified jet. That is the process

$$\text{“}\gamma\text{”} + p \rightarrow \text{jet}(x_j, k) + X$$

shown in Fig. 3 (or Fig. 2), where, for convenience, we denote the transverse momentum of the jet as simply $k \equiv k_{1T}$. The differential structure function for this process may be written in the form

$$x_j \frac{\partial F_2(x, Q^2; x_j, k^2)}{\partial x_j \partial k^2} = \frac{3\alpha(k^2)}{\pi k^4} \left(\sum_a x_j f_a(x_j, k^2)\right) F\left(\frac{x}{x_j}, k^2, Q^2\right) \quad (8)$$

[cf. Eq. (6)], where the sum over the parton distributions is given by Eq. (7). The factor F, which has the dimensions of k^2, represents the photon-gluon process shown by the upper blob in Fig. 3; that is F/k^2 can be identified with the gluon structure function integrated over the longitudinal momentum of the gluon. The factor k^{-4} in Eq. (8) arises from the gluon propagators. Since we are interested in small x/x_j, the magnitude of x_j should be taken as large as is experimentally feasible. In fact it has already been tacitly assumed in Eq. (8) [and Eq. (6)] that there is strong-ordering of the longitudinal momenta at the gluon-parton a vertex of Fig. 3 so that x_j of the exchanged parton, which occurs in $f_a(x_j, k^2)$, is to a good approximation that of the outgoing jet.

In the leading $\ln(x_j/x)$ approximation the structure function $F(x/x_j, k^2, Q^2)$ is given by the sum of ladder diagrams shown in Fig. 4, together with virtual gluon corrections (not shown). This gives a Lipatov equation for $F(z, k^2, Q^2)$ of the usual form

$$F(z,k^2,Q^2) = F_0(z,k^2,Q^2) + \frac{3\alpha_s}{\pi} k^2 \int_z^1 \frac{dz'}{z'} \int_0^\infty \frac{dk'^2}{k'^2} \left(\frac{F(z',k'^2,Q^2) - F(z,k^2,Q^2)}{|k'^2 - k^2|} + \frac{F(z,k^2,Q^2)}{(4k'^4 + k^4)^{\frac{1}{2}}} \right), \quad (9)$$

where the occurrence of $F(z, k^2, Q^2)$ in the integrand is on account of the diagrams with virtual corrections. In Eq. (9) the coupling is fixed at $\alpha_s(Q^2)$; we will discuss the effect of allowing α_s to run in the ladder integrations later.

The inhomogeneous or driving term F_0 in Eq. (9) corresponds to the sum of the quark box and crossed-box diagrams of Fig. 5, shown simply as a box in Fig. 4. For transversely polarized photons F_0 is found, for small z, to be

$$F_0(z,k^2,Q^2) \simeq F_0(0,k^2,Q^2) \equiv F_0(k^2,Q^2),$$

where

$$F_0(k^2,Q^2) = 2\sum_q e_q^2 \frac{Q^2}{4\pi^2} \alpha_s \int_0^1 d\beta \int_0^\infty d^2\kappa [\beta^2 + (1-\beta)^2] \times \left(\frac{\kappa^2}{[\kappa^2 + Q^2\beta(1-\beta)]^2} - \frac{\boldsymbol{\kappa}\cdot(\boldsymbol{\kappa} - \mathbf{k})}{[\kappa^2 + Q^2\beta(1-\beta)][(\boldsymbol{\kappa} - \mathbf{k})^2 + Q^2\beta(1-\beta)]} \right). \quad (10)$$

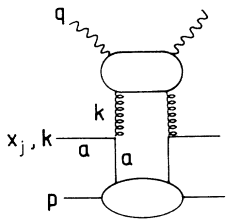

FIG. 3. The diagram giving the cross section for deep-inelastic scattering events containing an identified jet of longitudinal and transverse momentum $x_j p$ and k, respectively.

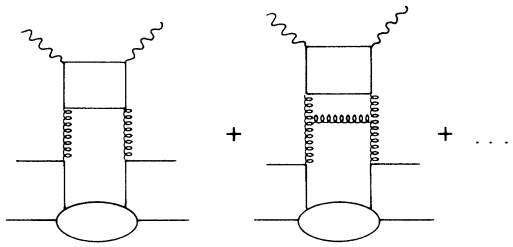

FIG. 4. The leading $\ln(x_j/x)$ approximation to the process shown in Fig. 3.

Equation (10) applies for arbitrary values of k^2 and Q^2, athough here we are interested in $k^2 \simeq Q^2$. In deriving Eq. (10) we have assumed massless quarks. We also neglect the small longitudinal contribution to F_2, so our results refer, in principle, to the structure function $2xF_1$ corresponding to transversly polarized virtual photons. For fixed α_s the relative smallness of $F_L = F_2 - 2xF_1$ has been checked [16], see below. The numerical results which we present in Sec. III are for values of Q^2 for which it is reasonable to assume that three quark flavors are active. We can rewrite the integrand of Eq. (10) in terms of a Feynman integral, which allows the $d^2\kappa$ integration to be performed analytically (see Appendix A). In this way we find

$$F_0(k^2,Q^2) = \frac{\sum e_q^2}{4\pi} k^2 Q^2 \alpha_s \int_0^1 d\beta \int_0^1 d\lambda \frac{[\lambda^2+(1-\lambda)^2][\beta^2+(1-\beta)^2]}{[\lambda(1-\lambda)k^2+\beta(1-\beta)Q^2]}. \tag{11}$$

As required, F_0 has the dimensions of k^2. Although here we are concerned with the regime where $k^2 \simeq Q^2$, we see from Eq. (11) that if $k^2 \ll Q^2$ then $F_0 \sim k^2$ modulo a $\ln(Q^2/k^2)$ factor; whereas if $k^2 \gg Q^2$ we have $F_0 \sim Q^2$, modulo a $\ln(k^2/Q^2)$ factor, which when inserted into Eq. (8) leads to the usual k^{-4} behavior associated with single jet production. The k^2 behavior of the driving term F_0 is not transmitted directly to F, but is significantly modified by the Lipatov equation [Eq. (9)] particularly at small z, as can be seen by inspection of Eq. (12) below, or from the discussion in Appendix B.

If, as we have so far assumed, the coupling α_s is fixed then we can use Mellin transform techniques [3–5] to solve the Lipatov equation (9) and obtain an analytic expression for the leading small-z behavior of $F(z,k^2,Q^2)$. Using these techniques on Eqs. (9) and (11) we find

$$F(z,k^2,Q^2) = \frac{9\pi^2}{512} \frac{2\sum e_q^2 \alpha_s^{\frac{1}{2}}}{\sqrt{21\zeta(3)/2}} \left(\frac{k^2}{Q^2}\right)^{\frac{1}{2}} Q^2 \frac{z^{-\alpha_P+1}}{\sqrt{\ln(1/z)}} \times \left[1+O\left(\frac{1}{\ln(1/z)}\right)\right] \tag{12}$$

with $\alpha_P - 1$ given by Eq. (5), and where ζ is the Riemann zeta function. The derivation of Eq. (12) is outlined in Appendix B. When this fixed coupling result is inserted into Eq. (8) we obtain the leading small $z \equiv x/x_j$ dependence that was forecast in Eq. (6). It is interesting to note that the k^2/Q^2 dependence shown in Eq. (12) arises because, in the fixed coupling case, the Mellin transform parameter r, conjugate to k^2, is equal to $\frac{1}{2}$ (as seen in Appendix B). The behavior is also related to the fact that the anomalous dimension $\gamma(n,\alpha_s)$ describing the k^2 evolution of the moments of F is equal to $\frac{1}{2}$ for $n = \alpha_P$ [17].

For the fixed coupling case the formula for the differential structure function [Eqs. (8) and (12)] has also been derived in Ref. [16]. They find that $F_L : 2xF_1$ are in the ratio 2 : 9.

The analytic approximation Eq. (12) will give at best a rough estimate of the value of $F(z,k^2,Q^2)$. For one thing, the Lipatov equation is based on perturbative QCD and so the transverse momenta of the exchanged gluons along the chains in Fig. 2 or Fig. 4 should satisfy $k^2 \gg \Lambda^2$, and so should be at least greater than 1 GeV^2 or so. This can be simply achieved by introducing a lower limit cutoff k_0^2 on the transverse momentum integral in Eq. (9). Second, we should allow the couplings α_s to depend on the transverse momenta along the ladder. The conventional way of introducing the k^2 or k'^2 dependence of α_s in Eq. (9) is to ensure that, if we were to revert to the strongly ordered case with $k^2 \ll Q^2$, we would recover the correct evolution equation in the double leading logarithm approximation with a running coupling. Following this procedure we find that the Lipatov equation for $F(z,k^2,Q^2)$ becomes

$$H(z,k^2,Q^2) = H_0(z,k^2,Q^2) + \frac{3\alpha_s(k^2)}{\pi} k^2 \int_z^1 \frac{dz'}{z'} \int_{k_0^2}^\infty \frac{dk'^2}{k'^2} \left(\frac{H(z',k'^2,Q^2)-H(z,k^2,Q^2)}{|k'^2-k^2|} + \frac{H(z,k^2,Q^2)}{(4k'^4+k^4)^{\frac{1}{2}}}\right) \tag{13}$$

with

$$H(z,k^2,Q^2) \equiv \frac{3\alpha_s(k^2)}{\pi} F(z,k^2,Q^2) \tag{14}$$

and similarly for H_0.

For consistency we should also study the sensitivity of the numerical results to the introduction of a transverse momentum cutoff in the determination of the driving term H_0 or F_0. To do this we write Eq. (10) in the form

$$F_0(k^2,Q^2) = \sum e_q^2 \frac{\alpha_s(k^2)}{\pi} k^2 Q^2 \int_0^1 d\beta \int_0^1 d\lambda \int_{\kappa_0^2}^{\infty} d\kappa'^2 [\beta^2 + (1-\beta)^2]\,\lambda \times \frac{(2\lambda-1)\kappa'^2 + (1-\lambda)[\lambda(1-\lambda)k^2 + \beta(1-\beta)Q^2]}{[\kappa'^2 + \lambda(1-\lambda)k^2 + \beta(1-\beta)Q^2]^3}. \quad (15)$$

The derivation of Eq. (15) is outlined in Appendix A.

In the next section we describe how we solve the Lipatov equation [Eq. (13)] numerically. We present results for deep-inelastic events with an identified jet for the choice of the transverse momenta cutoffs given by $k_0^2 = \kappa_0^2 = 1$ GeV^2 and we compare with those obtained from the approximate analytic expression, Eq. (12). We also investigate the sensitivity of the results to the choice of the value of the cutoffs.

III. NUMERICAL QCD ESTIMATES OF DEEP-INELASTIC + JET EVENTS

In Sec. II we described how the measurement of deep-inelastic scattering (x,Q^2) events which contain an identified jet (x_j,k^2), with $k^2 \sim Q^2$, is a particularly sensitive probe for investigating the small $z \equiv x/x_j$ behavior of the gluon $g(z,Q^2)$, free from having to assume an input distribution $g(z,Q_0^2)$. Certainly we would expect that measurements at HERA would be able to distinguish the singular Lipatov $z^{1-\alpha_P}$ form of growth, with decreasing z, that was shown in Eq. (12). The analytic expression, Eq. (12), is only an approximation for the leading small-z behavior of $F(z,k^2,Q^2)$ and to make a reliable quantitative estimate of deep-inelastic scattering with a measured jet we must solve the Lipatov equation, Eq. (13).

This integral equation (13) for $F(z,k^2,Q^2)$ is based on a leading $\ln(1/z)$ summation and so is not expected to be applicable beyond the small-z region. On the other hand, we anticipate that the inhomogeneous term $F_0(z,k^2,Q^2)$ itself should be a reasonable approximation to $F(z,k^2,Q^2)$ in the large-z region, particularly for the $k^2 \sim Q^2$ values that we are studying. This follows because the standard Altarelli-Parisi QCD evolution should be applicable in this region and when $k^2 \simeq Q^2$ the evolution length $[\sim \alpha_s \ln(Q^2/k^2)]$ is very small so that the effects of evolution can be safely neglected. We can therefore restrict the study of the Lipatov equation (13) to the small-z region, $z < z_0$, by imposing the boundary condition

$$F(z_0,k^2,Q^2) \simeq F_0(z_0,k^2,Q^2) = F_0(k^2,Q^2), \quad (16)$$

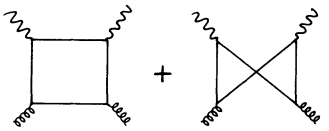

FIG. 5. The two diagrams embodied in the quark box diagram of Fig. 4 .

where z_0 is chosen sufficiently small so that Eq. (11) is a reasonable approximation for F_0. This means we can solve the Lipatov equation (13) by writing it in the form of an integrodifferential equation

$$z\frac{\partial H}{\partial z} = K \otimes H, \quad (17)$$

where K is the kernel and $\otimes$ denotes the integration over k'^2. We impose the boundary conditions

$$H(z_0,k^2,Q^2) = H_0(k^2,Q^2)$$

and choose $z_0 = 0.1$. For any small z the solution $H(z,k^2,Q^2)$ therefore only depends on the behavior of H in the interval (z,z_0).

Using this procedure we obtain the results shown in Fig. 6. To be precise the continuous curves are the values of $F(z,k^2,Q^2)$ determined by solving Eq. (17) using three different values of the transverse momentum cutoff, namely $k_0^2 = 1$, 2, and 4 GeV^2. For comparison, the dashed curve is the approximate analytic form [Eq. (12)] shown as $F(z/z_0,k^2,Q^2)$ as a function of z, which cor-

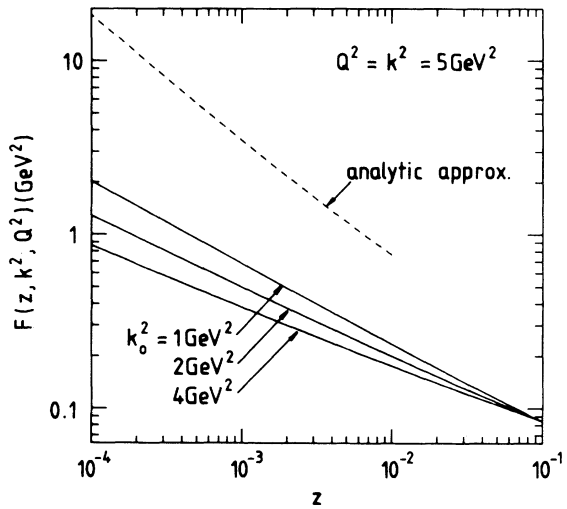

FIG. 6. The photon-gluon structure function factor $F(z,k^2,Q^2)$ which controls, via Eq. (8), the strength of the differential structure function for deep-inelastic (x,Q^2) events with an identified jet (x_j,k^2), as a function of $z = x/x_j$. The continuous curves are calculated from the integrodifferential form Eq. (17) of the Lipatov equation Eq. (13) for three different choices of the transverse momentum cutoff, $k_0^2 = 1$, 2 and 4 GeV^2, respectively. The solution is matched to the quark-box driving term F_0 at $z = z_0 = 0.1$. The dashed curve shows, for comparison, the analytic leading $\ln(z_0/z)$ approximation, Eq. (12), for $F(z/z_0,k^2,Q^2)$. Here we take $\kappa_0^2 = 1$ GeV^2 in Eq. (15).

responds to the leading $\ln(z_0/z)$ behavior of the Lipatov equation with fixed coupling $\alpha_s(Q^2)$ and with the boundary condition $F = F_0$ at $z = z_0$. This asymptotic form is of course not valid for $z \simeq z_0$ and so is only shown in Fig. 6 for $z/z_0 < 0.1$.

Several features of Fig. 6 are worth noting. First, the $z^{1-\alpha_P}$ behavior of F soon emerges from the integrodifferential equation as z decreases from z_0. As expected the slope $1 - \alpha_P$ is sensitive to the choice of the transverse momentum cutoff and is, in fact, controlled by the value of $\alpha_s(k_0^2)$. The "asymptotic" values of the slopes of the curves in Fig. 6 for the cutoff choices $k_0^2 = 1$, 2, and 4 GeV^2 correspond to $\alpha_P - 1 = 0.48$, 0.42, and 0.38 respectively. These are in complete agreement with the behavior of the solutions of a Lipatov equation for the gluon distribution itself which were presented in Ref. [7]. Second we see from Fig. 6 that the approximate analytic form for F substantially overestimates the numerical solutions and, in particular, that it has a steeper form with decreasing z. The reason is a little subtle. The (negative) slope, $\alpha_P - 1$, at very small z can be directly identified with the maximum eigenvalue of the kernel of the Lipatov equation (see, for example, Ref. [6] for a simplified explanation). In the fixed coupling case the leading eigenvalue $\alpha_P - 1$ is given by Eq. (5) with $\alpha_s = \alpha_s(Q^2)$. In the more realistic running coupling case the maximum eigenvalue is controlled by $\alpha_s(k_0^2)$ and, since all the chosen cut-offs k_0^2 are less than Q^2, we would at first sight expect the continuous curves to have steeper slopes than the dashed "fixed coupling" curve. However it turns out that the coefficient of $\alpha_s(k_0^2)$ in the running coupling case is numerically much smaller (and dependent on k_0^2) than the coefficient $12\ \ln 2/\pi$ of the fixed α_s occurring in Eq. (5).

We are now in a position to show our main result, which is the behavior of the differential structure function, $\partial F_2/\partial x_j\, \partial k^2$, for deep-inelastic (x, Q^2) events containing a measured jet (x_j, k^2) as a function of x and x_j for fixed values of k^2 and Q^2. We evaluate Eq. (8) using the values of $F(x/x_j, k^2, Q^2)$ obtained for $k_0^2 = \kappa_0^2 = 1$ GeV^2 and with $\sum f_a$ calculated from the g, q and $\bar{q}$ parton distributions of set B_- of Kwiecinski, Martin, Roberts, and Stirling (KMRS) [6]. The results are shown by the continuous curves in Fig. 7 as a function of x_j for different values of x where in the upper figure $k^2 = Q^2 = 5$ GeV^2 while in the lower figure the jet transverse momentum k is increased to $k^2 = 10$ GeV^2.

For comparison we also plot in Fig. 7 (as a dashed curve) the approximation where the full solution for $F(x/x_j, k^2, Q^2)$ is replaced in Eq. (8) simply by the quark-box driving term $F_0(x/x_j, k^2, Q^2)$. The difference between the continuous and dashed curves for the differential structure function (i.e., inputting F versus F_0) is the Lipatov effect. The input $F_0(z, k^2, Q^2)$ for the dashed curves is independent of z and the x_j dependence is entirely due to that of the quark and gluon distributions in the proton, whereas the continuous curves also embody the rapid "Lipatov" increase of $F(z, k^2, Q^2)$ with increasing $z = x/x_j$. Inspection of Fig. 7 shows that the

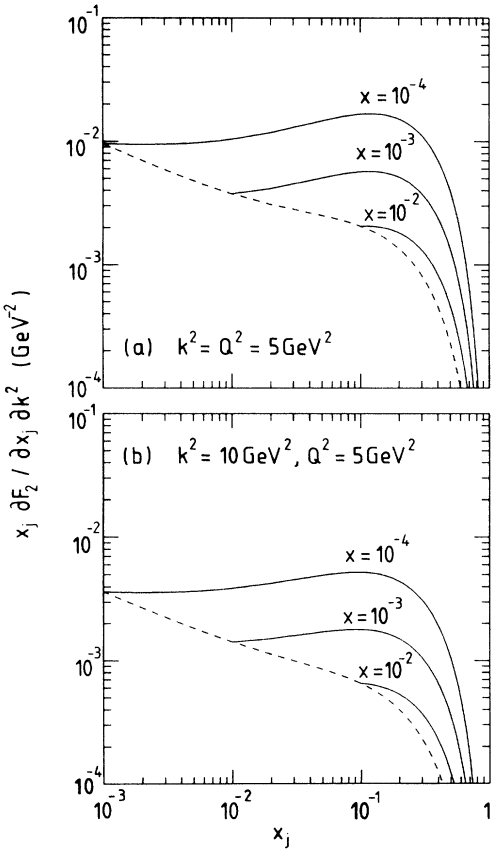

FIG. 7. The differential structure function, Eq. (8), for deep-inelastic (x, Q^2) events with an identified jet (x_j, k^2) as a function of x_j for different values of x, $x = 10^{-4}$, 10^{-3}, and 10^{-2}, and for $Q^2 = 5$ GeV^2. The dashed curve is obtained from Eq. (8) with F replaced by simply the driving term F_0. The cutoffs are chosen to be $k_0^2 = \kappa_0^2 = 1$ GeV^2. (a) and (b) correspond to jet transverse momentum squared $k^2 = 5$ and 10 GeV^2, respectively.

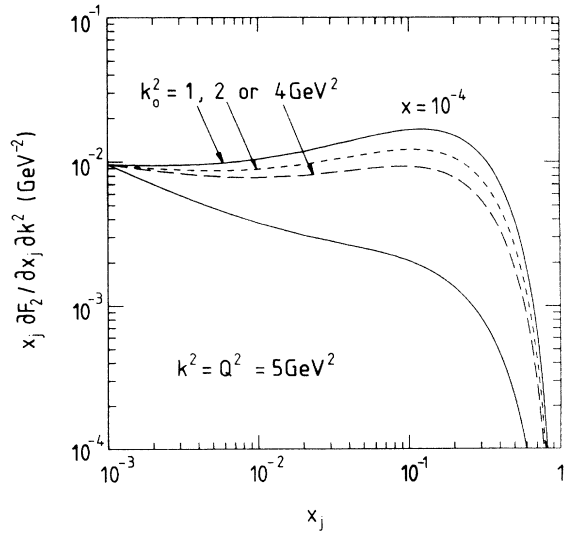

FIG. 8. The sensitivity of the QCD predictions of the differential structure function Eq. (8) to the choice of the cutoff k_0^2 of Eq. (13). The lower curve, shown for reference, is for F replaced by F_0 in Eq. (8). Here we take $\kappa_0^2 = 1$ GeV^2 in Eq. (15).

difference is dramatic, particularly at small x ($x \lesssim 10^{-3}$), in the region around $x_j \sim 0.1$–0.2. As was explained below Eq. (8), the magnitude of x_j should be of this order for our formalism to be valid. That is the results of Fig. 7 are only expected to be reliable for $x_j \gtrsim 0.05$.

It would be tempting to conclude that measurements of deep-inelastic scattering events with an identified jet can reveal the QCD singular Lipatov behavior from observing either the shape or the magnitude of $\partial F_2/\partial x_j\,\partial k^2$. However the (x_j, x) shape is a more reliable discriminator than the magnitude since, as we shall show, the normalization of the QCD predictions is subject to uncertainties arising mainly from the choice of the cutoffs in the integrations over the transverse momenta. First we show in Fig. 8 the dependence of the results to the choice of the cutoff k_0^2 in Eq. (13) [or Eq. (17)]. We give predictions for $k_0^2 = 1$, 2 and 4 GeV^2. Although the choice $k_0^2 = 4$ GeV^2 is extreme, the uncertainty in normalization is apparent. We now turn to the effect of the cutoff ambiguity in the calculation of the driving term F_0. Figure 9 shows results for the cutoff choices $\kappa_0^2 = 0$, 1, and 2 GeV^2 in the transverse momentum integration of Eq. (15). Again we see a substantial change in normalization but very little effect on the shape of the differential structure function.

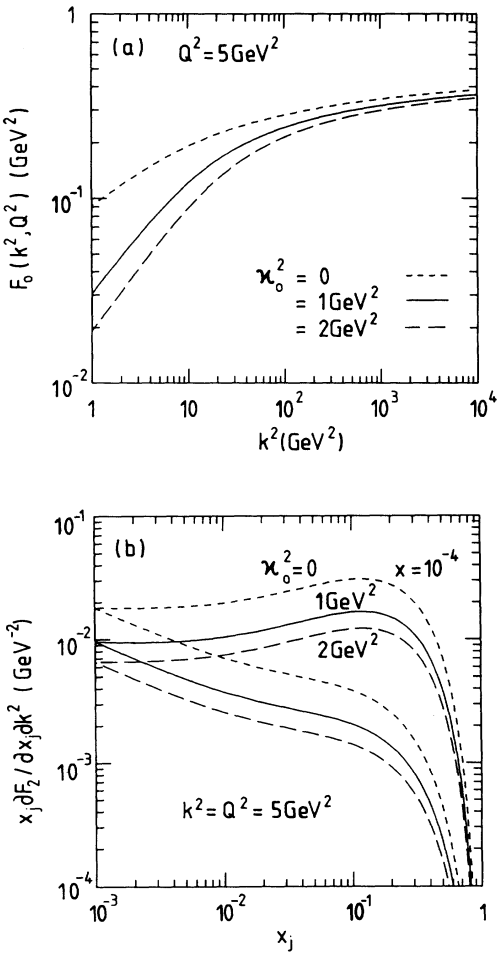

FIG. 9. (a) The quark-box "driving term" $F_0(k^2, Q^2)$ of Eq. (15) calculated as a function of k^2 for three different values of the cutoff, namely $\kappa_0^2 = 0$, 1 and 2 GeV^2. (b) The forms of the differential structure function Eq. (8) obtained with F calculated using the three forms of F_0 shown in (a). The three lower curves in (b) are obtained from Eq. (8) when F is replaced by F_0.

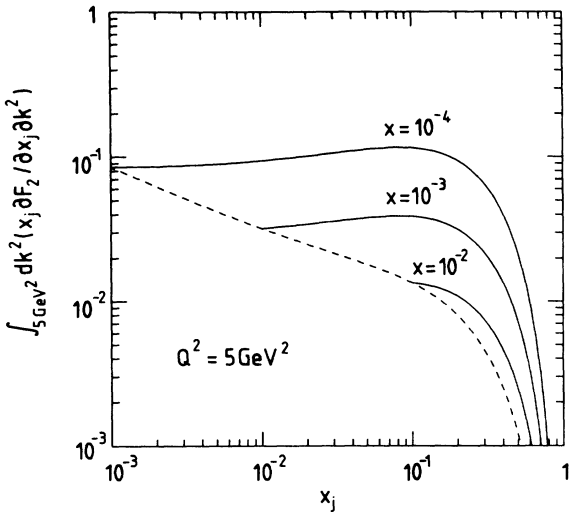

FIG. 10. The differential function for deep-inelastic (x, Q^2) events with a measured jet (x_j, k^2) with transverse momentum squared $k^2 > 5$ GeV^2, shown as a function of x_j for three values of x. The cutoffs are chosen to be $k_0^2 = \kappa_0^2 = 1$ GeV^2. The dashed curve, shown for reference, is obtained from Eq. (8) when F is replaced by F_0.

Figure 10 shows the QCD predictions for the differential structure function for deep-inelastic scattering with an identified jet with transverse momentum squared $k^2 > 5$ GeV^2 as a function of x_j for different values of x. That is Eq. (8) integrated over k^2 from 5 GeV^2 upwards. If we then carry out the integration over x_j we would find the fraction of such events in relation to an inclusive deep-inelastic measurement of F_2. For example, from Fig. 10 we find at $x = 10^{-3}$ (and $Q^2 = 5$ GeV^2) that the doubly integrated structure function

$$F_2^{jet}(x, Q^2; x_j > 0.05, k^2 > 5\ \text{GeV}^2) = 0.071$$

as compared to the KMRS (set B_-) prediction of $F_2(x, Q^2) = 0.32$, that is an order-of-magnitude reduction as would be expected for an $O(\alpha_s)$ subprocess. We should keep in mind however, that the normalization of F_2^{jet} has a large uncertainty (of order a factor of 2 either way) arising from the sensitivity of the QCD prediction to the choice of the values of the cutoffs, k_0^2 and κ_0^2, on the integrals over the transverse momenta.

IV. SUMMARY

In this paper we have studied the proposal that the measurement of the jet electroproduction spectrum in the small-x region allows a unique probe of the novel QCD effects which are expected to occur in this region.

Indeed such an experiment offers a particularly clean way to reveal the QCD (Pomeron) singularity implied by the leading $\ln(1/x)$ resummation. The measurement has a different character from, and is complementary to, the other proposed experimental probes of the small-x behavior of the parton distributions such as heavy quark [13,18, 19] and J/ψ [20] electroproduction, prompt photon production [19] and ordinary inclusive deep-inelastic lepton-nucleon scattering. Although such direct measurements of parton distributions are extremely valuable, it will be difficult to use them to unambiguously identify the genuine Lipatov QCD growth with decreasing x. The reason is that these processes (a) involve evolution in Q^2 which steepens the small-x parton behavior with increasing Q^2 and (b) require us to assume some input form of the parton distributions, $f_a(x, Q_0^2)$ (with, say, $Q_0^2 = 4$ GeV^2), which contain nonperturbative effects. Thus we cannot be sure whether an observed steep small-x behavior is due to a combination of our input assumptions and the Q^2 evolution or is indeed a genuine Lipatov perturbative QCD effect.

The unique feature of the measurement of deep-inelastic (x, Q^2) events containing an identified jet (x_j, k^2) is the potential possibility of eliminating the effect of the conventional QCD evolution by choosing $k^2 \simeq Q^2$ and to cleanly isolate the small x/x_j behavior directly at the *partonic* level. Recall from our discussion in Sec. I that, since

$$\left(\frac{x_j}{x}\right) Q^2 \simeq s_{\gamma a},$$

small x/x_j is directly linked to the high c.m. energy $\sqrt{s_{\gamma a}}$ behavior of a *partonic* subprocess, that is the virtual-photon–virtual-parton-a subprocess in Fig. 3. A similar kinematical *parton* configuration can, in principle, be achieved in dijet production in hadronic collisions [16], but the study of single jets in *ep* collisions should be experimentally much more accessible, particularly with the advent of HERA.

We found that the singular small-x Lipatov effects dramatically modify both the shape and the normalization of the jet spectrum in *ep* collisions (see, for example, the difference between the continuous and dashed curves in Fig. 7). The overall normalization is found to be subject to ambiguities related to the choice of the low transverse momentum cutoff. It is here that nonperturbative effects enter our study and lead to some uncertainty in the exponent of the QCD singular $z^{1-\alpha_P}$ behavior with, for different choices of the cutoff, $\alpha_P - 1$ ranging from about 0.35 to 0.5. However the shape of the jet spectrum is much less sensitive to the choice of the cut-offs and so such measurements should serve as an ideal means of identifying the QCD small-x behavior.

We also derived a closed analytic form Eq. (12), advocated in Ref. [14], which corresponds to the solution of the Lipatov equation with fixed coupling $\alpha_s(Q^2)$ and with no lower cut-off on the transverse momentum. This approximation is found to grossly overestimate the jet yield.

So far we have neglected shadowing corrections. The rapid growth of the photon-virtual gluon subprocess in Fig. 3 with decreasing x/x_j cannot go on indefinitely, but must ultimately be suppressed by shadowing or recombination effects. These shadowing corrections in the photon–virtual-gluon channel preserve the factorization-like form [Eq. (8)] of the differential structure function $x_j\,\partial F_2/\partial x_j\,\partial k^2$. The corrections give rise to nonlinear terms in the integrodifferential equation (13) for H which would slow the rapid growth of $F(z, k^2, Q^2)$ with decreasing z.

Conceptually these effects are the same as the shadowing contributions which occur in another process, one for which we have some experience, namely the shadowing corrections to the gluon structure function $g(x, Q^2)$ itself. In this case the rapid rise, with decreasing x, is in the virtual-gluon–proton channel, and the suppression is found [6,7] to be small for $x \gtrsim 10^{-3}$. We would therefore expect that the QCD predictions that we have shown, for which $z \equiv x/x_j > 10^{-3}$, will have negligible corrections for shadowing in the photon–virtual-gluon channel. Of course it is possible that shadowing will be more complicated, and even spoil the factorization structure of Eq. (8), but it is unlikely that it will significantly distort the shape of the jet spectrum in the region $x/x_j \gtrsim 10^{-3}$ accessible to HERA.

We conclude that measurements of deep-inelastic (x, Q^2) events accompanied by an identified jet (x_j, k^2), with $k^2 \simeq Q^2$, will provide a clean and unique way of investigating the Lipatov perturbative QCD growth expected at small $z = x/x_j$. This QCD landmark measurement should be possible at HERA by studying the shape of the jet spectrum as a function of x and x_j in the region $x \sim 10^{-3}$ and $x_j \sim 0.1$.

ACKNOWLEDGMENTS

We thank Al Mueller and Dick Roberts for stimulating our interest in this problem. One of us (J.K.) thanks the Physics Department and Grey College of the University of Durham for their warm hospitality, and another (P.J.S.) thanks SERC for financial support. J.K. was supported in part by the Polish Committee for Scientific Research (Grant No. 2 0198 91 01).

APPENDIX A

Here we show how to write the basic box-diagram formula (10) for the driving term, first, in the form of Eq. (11), which is suitable for deriving an analytic result for the (transverse part of the) differential structure function in the fixed coupling case, and second in the form of Eq. (15), which is suitable for studying the sensitivity of the numerical results to the value of the cutoff κ_0^2 on the integration over the transverse momentum. The trick is to use the standard Feynman integral to rewrite the integrand of the $d^2\kappa$ integration in Eq. (10) in the form

$$\left(\frac{\kappa^2}{[\kappa^2+Q^2\beta(1-\beta)]^2}-\frac{\boldsymbol{\kappa}\cdot(\boldsymbol{\kappa}-\mathbf{k})}{[\kappa^2+Q^2\beta(1-\beta)][(\boldsymbol{\kappa}-\mathbf{k})^2+Q^2\beta(1-\beta)]}\right)$$

$$=2\int_0^1 d\lambda\,\lambda\frac{\kappa^2[(\boldsymbol{\kappa}-\mathbf{k})^2+Q^2\beta(1-\beta)]-\boldsymbol{\kappa}\cdot(\boldsymbol{\kappa}-\mathbf{k})[\kappa^2+Q^2\beta(1-\beta)]}{[\lambda\kappa^2+(1-\lambda)(\boldsymbol{\kappa}-\mathbf{k})^2+Q^2\beta(1-\beta)]^3}. \quad \text{(A1)}$$

By replacing the transverse momentum variable κ by

$$\boldsymbol{\kappa} = \boldsymbol{\kappa}'+(1-\lambda)\mathbf{k} \quad \text{(A2)}$$

we can eliminate the angular dependence and reduce the twofold integration $d^2\kappa$ to the single integration $\pi\,d\kappa'^2$. Equation (10) then becomes

$$F_0(k^2,Q^2)=\sum e_q^2\frac{\alpha_s(k^2)}{\pi}k^2\,Q^2\int_0^1 d\beta\int_0^1 d\lambda\int_0^\infty d\kappa'^2[\beta^2+(1-\beta)^2]\,\lambda \times\frac{(2\lambda-1)\kappa'^2+(1-\lambda)[\lambda(1-\lambda)k^2+\beta(1-\beta)Q^2]}{[\kappa'^2+\lambda(1-\lambda)k^2+\beta(1-\beta)Q^2]^3} \quad \text{(A3)}$$

which after integrating over κ'^2 leads to formula Eq. (11) for F_0. A related formula may be found in Ref. [21]. Imposing a lower limit cutoff κ_0^2 on the integration in Eq. (A3) gives Eq. (15) of Sec. II.

APPENDIX B

In the fixed coupling case we can solve the Lipatov equation Eq. (9) to obtain an analytic expression for the leading small-z behavior of $F(z,k^2,Q^2)$. The result is formula Eq. (12) of Sec. II and is derived as follows. First we introduce the moment function $\bar{F}(n,...)$ of $F(z,...)$ defined by

$$\bar{F}(n,k^2,Q^2) = \int_0^1 dz\,z^{n-2}F(z,k^2,Q^2), \quad \text{(B1)}$$

and conversely

$$F(z,k^2,Q^2)=\frac{1}{2\pi i}\int_{c-i\infty}^{c+i\infty} dn\,z^{-n+1}\bar{F}(n,k^2,Q^2), \quad \text{(B2)}$$

where the integration contour in Eq. (B2) is located to the right of the singularities of $\bar{F}$ in n. In terms of the moment function, the Lipatov equation, Eq. (9), reduces to an integral equation in a single variable

$$\bar{F}(n,k^2,Q^2)=\frac{F_0(k^2,Q^2)}{n-1}+\frac{3\alpha_s}{\pi(n-1)}k^2\int_0^\infty\frac{dk'^2}{k'^2}\left(\frac{\bar{F}(n,k'^2,Q^2)-\bar{F}(n,k^2,Q^2)}{|k'^2-k^2|}+\frac{\bar{F}(n,k^2,Q^2)}{(4k'^4+k^4)^{\frac{1}{2}}}\right). \quad \text{(B3)}$$

This equation can be solved by taking the Mellin transform $\tilde{F}(\cdots r\cdots)$ of $\bar{F}(\cdots k^2\cdots)$

$$\tilde{F}(n,r,Q^2) = \int_0^\infty dk^2(k^2)^{-r-1}\bar{F}(n,k^2,Q^2) \quad \text{(B4)}$$

which gives [3, 16]

$$\tilde{F}(n,r,Q^2) = \frac{\tilde{F}_0(r,Q^2)}{n-1-(3\alpha_s/\pi)\tilde{K}(r)}, \quad \text{(B5)}$$

where $\tilde{K}$ is the Mellin transform of the kernel of the integral equation Eq. (B3), that is

$$\tilde{K}(r) = -[\Psi(r)+\Psi(1-r)-2\Psi(1)], \quad \text{(B6)}$$

where Ψ is the logarithmic derivative of the Euler gamma function: $\Psi(z)\equiv\Gamma'(z)/\Gamma(z)$. The function $\tilde{F}_0(r,Q^2)$ is the Mellin transform of the driving term $F_0(k^2,Q^2)$. Using Eq. (11) for $F_0(k^2,Q^2)$ and performing the k^2 integration we find

$$\tilde{F}_0(r,Q^2)=\frac{\alpha_s\sum e_q^2}{4\sin\pi r}(Q^2)^{1-r}\int_0^1 d\lambda[\lambda^2+(1-\lambda)^2][\lambda(1-\lambda)]^{r-1}\int_0^1 d\beta[\beta^2+(1-\beta)^2][\beta(1-\beta)]^{-r}$$
$$=\frac{\alpha_s\sum e_q^2}{\sin\pi r}(Q^2)^{1-r}B(r+2,r)B(3-r,1-r), \quad \text{(B7)}$$

where $B(a,b)$ is the Euler beta function. Finally, to obtain $F(z,k^2,Q^2)$ we must calculate the double inverse of solution Eq. (B5), that is

$$F(z,k^2,Q^2)=\left(\frac{1}{2\pi i}\right)^2\int_{c-i\infty}^{c+i\infty}dn\,z^{-n+1}\int_{\frac{1}{2}-i\infty}^{\frac{1}{2}+i\infty}dr(k^2)^r\frac{\tilde{F}_0(r,Q^2)}{n-1-(3\alpha_s/\pi)\tilde{K}(r)}. \quad \text{(B8)}$$

Performing the n integration and changing the other integration variable r to $\frac{1}{2}+i\nu$ we obtain

$$F(z,k^2,Q^2)=\frac{1}{2\pi}\int_0^\infty d\nu\left[(k^2)^{\frac{1}{2}+i\nu}\tilde{F}_0(\tfrac{1}{2}+i\nu,Q^2)+(k^2)^{\frac{1}{2}-i\nu}\tilde{F}_0(\tfrac{1}{2}-i\nu,Q^2)\right]z^{-(3\alpha_s/\pi)\tilde{K}(\frac{1}{2}+i\nu)}. \quad \text{(B9)}$$

Now it follows from Eq. (B6) that the function $\tilde{K}(\frac{1}{2}+i\nu)$ is maximum at $\nu=0$ and decreases with increasing ν. Thus the leading small-z behavior of F is controlled by the contribution near $\nu=0$. Expanding about this point we find

$$F(z,k^2,Q^2) = \frac{1}{\pi}(k^2)^{\frac{1}{2}}\tilde{F}_0(r=\tfrac{1}{2},Q^2)z^{1-\alpha_P} \times \int_0^\infty d\nu \exp\left(-\frac{3\alpha_s}{2\pi}\tilde{K}''(r=\tfrac{1}{2})\ln(1/z)\nu^2\right) \times \left[1+O\left(\frac{1}{\ln(1/z)}\right)\right] \quad \text{(B10)}$$

where

$$\alpha_P - 1 = \frac{3\alpha_s}{\pi}\tilde{K}(r=\tfrac{1}{2}) = \frac{12\alpha_s}{\pi}\ln 2, \quad \text{(B11)}$$

as in Eq. (5). If we now perform the integration over the Gaussian form in ν, evaluate $\tilde{F}_0(\frac{1}{2},Q^2)$ from Eq. (B7) and note that $\tilde{K}''(\frac{1}{2}) = 28\zeta(3)$, then we obtain the leading small-z behavior,

$$F(z,k^2,Q^2) = \frac{9\pi^2}{512}\frac{2\sum e_q^2\alpha_s^{\frac{1}{2}}}{\sqrt{21\zeta(3)/2}}\left(\frac{k^2}{Q^2}\right)^{\frac{1}{2}}Q^2\frac{z^{1-\alpha_P}}{\sqrt{\ln(1/z)}}, \quad \text{(B12)}$$

that was quoted in Eq. (12).

[1] *Proceedings of the Topical Workshop on the Small-x Behavior of Deep Inelastic Scattering Structure Functions in QCD*, Hamburg, Germany, 1990, edited by A. Ali and J. Bartels [Nucl. Phys. B (Proc. Suppl.) **18C** (1990)]; E.M. Levin, Orsay Report No. LPTHE 91/02, 1991 (unpublished); DESY Report No. 91-110, 1991 (unpublished); A.D. Martin, in *Parton Distributions*, Proceedings of the Cracow School of Theoretical Physics, Zakopane, Poland, 1991 [Acta Phys. Pol. B **22**, 1095 (1991)].

[2] G. Altarelli and G. Parisi, Nucl. Phys. **B126**, 298 (1977); see also Yu.L. Dokshitzer, Zh. Eksp. Teor. Fiz. **73**, 1216 (1977) [Sov. Phys. JETP **46**, 641 (1977)]; V.N. Gribov and L.N. Lipatov, Yad. Fiz. **15**, 137 (1972) [Sov. J. Nucl. Phys. **15**, 79 (1972)].

[3] E.A. Kuraev, L.N. Lipatov, and V.S. Fadin, Zh. Eksp. Teor. Fiz. **72**, 377 (1977) [Sov. Phys. JETP **45**, 199 (1977)]; Ya.Ya. Balitsky and L.N. Lipatov, Yad. Fiz. **28**, 1597 (1978) [Sov. J. Nucl. Phys. **28**, 822 (1978)]; J.B. Bronzan and R.L. Sugar, Phys. Rev. D **17**, 585 (1978); T. Jaroszewicz, Acta. Phys. Pol. B **11**, 965 (1980); M. Ciafaloni, Nucl. Phys. **B296**, 49 (1988); S. Catani, F. Fiorani, and G. Marchesini, Phys. Lett. B **234**, 339 (1990); Nucl. Phys. **B336**, 18 (1990).

[4] L.V. Gribov, E.M. Levin, and M.G. Ryskin, Phys. Rep. **100**, 1 (1983).

[5] L.V. Gribov, E.M. Levin, and M.G. Ryskin, Nucl. Phys. **B188**, 155 (1981); Zh. Eksp. Teor. Fiz. **80**, 2132 (1981) [Sov. Phys. JETP **53**, 1113 (1981)]; A.H. Mueller and J. Qiu, Nucl. Phys. **B268**, 427 (1986); A.H. Mueller, *ibid.* **B335**, 115 (1990).

[6] J. Kwiecinski, A.D. Martin, R.G. Roberts, and W.J. Stirling, Phys. Rev. D **42**, 3645 (1990).

[7] J. Kwiecinski, A.D. Martin, and P.J. Sutton, Phys. Lett. B **264**, 199 (1991); Phys. Rev. D **44**, 2640 (1991).

[8] J. Bartels, J. Blümlein, and G. Schuler, Z. Phys. C **50**, 91 (1991).

[9] J. Bartels, Particle World **2**, 46 (1991).

[10] *Proceedings of the DESY Workshop 1987: Physics at HERA*, Hamburg, Germany, 1987, edited by R.D. Peccei (Deutsches Elektronen Synchrotron, Hamburg, 1988).

[11] J. Kwiecinski, Z. Phys. C **29**, 561 (1985); M. Krawczyk, in *Proceedings of the Topical Workshop on the Small-x Behavior of Deep Inelastic Structure Functions in QCD* [1], p. 64; K. Charchula and M. Krawczyk, DESY Report No. 90-122, 1990 (unpublished).

[12] G. Marchesini and B.R. Webber, Nucl. Phys. **B349**, 617 (1991); E.M. Levin, G. Marchesini, M.G. Ryskin, and B.R. Webber, *ibid.* **B357**, 167 (1991).

[13] B.R. Webber, Cavendish Report No. HEP-91/9 (unpublished).

[14] A.H. Mueller, in *Proceedings of the Topical Workshop on the Small-x Behavior of Deep Inelastic Structure Functions in QCD* [1], p. 125; J. Phys. G **17**, 1443 (1991).

[15] A.H. Mueller and H. Navelet, Nucl. Phys. **B282**, 727 (1987).

[16] J. Bartels, A. De Roeck, and M. Loewe, Z. Phys. C (to be published); W.-K. Tang, Phys. Lett. B **278**, 363 (1992); S. Catani, M. Ciafaloni, and F. Hautmann, in Proceedings of the Workshop on Physics at HERA, Hamburg, Germany, 1991, edited by W. Buchmüller and G. Ingelman (unpublished).

[17] T. Jaroszewicz, Phys. Lett. **116B**, 291 (1982).

[18] S. Catani, M. Ciafaloni, and F. Hautmann, Phys. Lett. B **242**, 97 (1990); Nucl. Phys. **B366**, 135 (1991); J.C. Collins and R.K. Ellis, *ibid.* **B360**, 3 (1991); B.R. Webber, in Proceedings of the Workshop on Physics at HERA [16].

[19] R.K. Ellis and D.A. Ross, Nucl. Phys. **B345**, 79 (1990).

[20] A.D. Martin, C.-K. Ng, and W.J. Stirling, Phys. Lett. B **191**, 200 (1987); Z. Kunszt, *ibid.* **207**, 103 (1988); K.J. Abraham, *ibid.* **240**, 224 (1990).

[21] L.N. Lipatov, in *Perturbative QCD*, edited by A.H. Mueller (World Scientific, Singapore, 1989), p. 411.